Design Study of Beam Dynamics Issues For 1 TeV Next Linear Collider Based Upon the Relativistic-Klystron Two-Beam Accelerator*

H. Li[1], T. Houck[2], N. Goffeney[1], E. Henestroza[1],
A. Sessler[1], G. Westenskow[2] and S. Yu[1]

[1]Lawrence Berkeley Laboratory
One Cyclotron Road, Berkeley, California 94720

[2]Lawrence Livermore National Laboratory
P.O. Box 808, Livermore, California 94550

November 1, 1994

MASTER

DISCLAIMER

Portions of this document may be illegible in electronic image products. Images are produced from the best available original document.

Design Study of Beam Dynamics Issues For 1 TeV Next Linear Collider Based Upon the Relativistic-Klystron Two-Beam Accelerator*

H. Li[1], T. Houck[2], N. Goffeney[1], E. Henestroza[1],
A. Sessler[1], G. Westenskow[2] and S. Yu[1]

[1] Lawrence Berkeley Laboratory
One Cyclotron Road, Berkeley, California 94720

[2] Lawrence Livermore National Laboratory
P.O. Box 808, Livermore, California 94550

Abstract. A design study has recently been conducted for exploring the feasibility of a relativistic-klystron two-beam accelerator (RK-TBA) system as a rf power source for a 1 TeV linear collider. We present, in this paper, the beam dynamics part of this study. We have achieved in our design study acceptable transverse and longitudinal beam stability properties for the resulting high efficiency and low cost RK-TBA.

1. INTRODUCTION

The two-beam accelerator (TBA) (Figure 1) concept has been studied quite extensively over the past ten years[1-2]. Many theoretical papers were written on this subject[3-7], and high power extraction through free-electron laser and relativistic klystron devices were demonstrated in earlier experiments[8-9]. Quite recently, reacceleration was demonstrated experimentally[10], where a bunched beam was successfully transported through three traveling wave extraction cavities and two intervening reacceleration units (Figure 2) for a total rf output of about 200 MW. The amplitude and phase were shown to be stable over a significant portion of the beam pulse (Figure 3a and 3b).
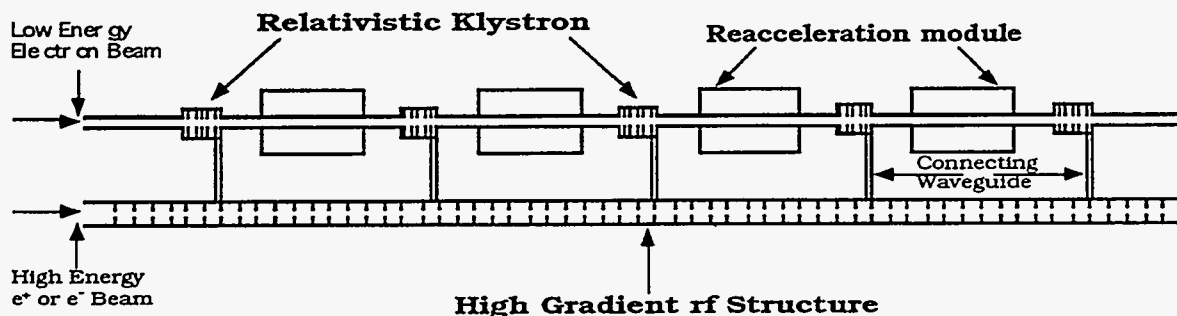

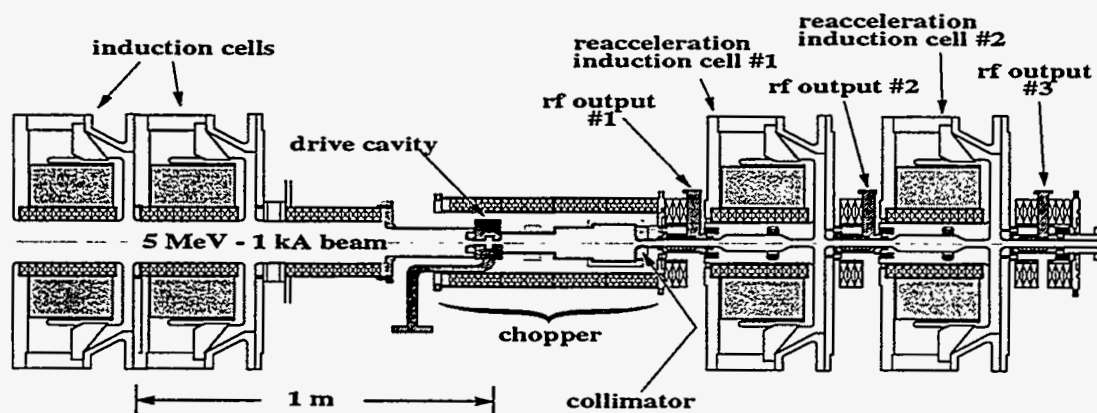**FIGURE 1.** Schematic of TBA scheme of Relativistic Klystron version.

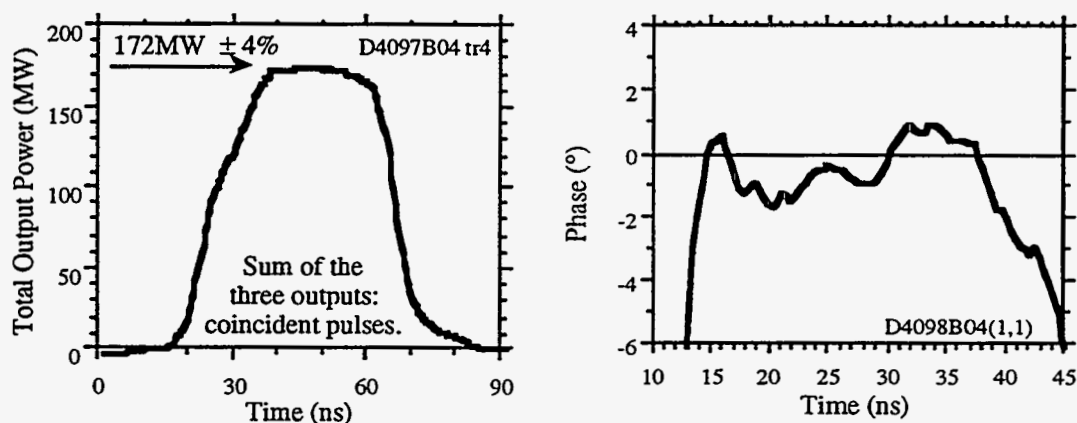**FIGURE 2.** Layout of reacceleration experiments at LLNL.

FIGURE 3. (a) Amplitude and (b) Phase stability of the power pulse for Fig. 2.

In the design and performance of these as well as previous experiments, longitudinal and transverse beam dynamics codes, RKS[11] and OMICE[12], were developed and checked, and the numerical results were shown to be in overall agreement with that of the experiments.

Encouraged by this progress, we have recently embarked on a systems study to revisit the practicality of the TBA as a realistic power source candidate for a 1 TeV Next Linear Collider (NLC)[13]. The preliminary system design study is reported elsewhere[14]. In this paper, we focus on the beam dynamics issues, using as study tools the same computer codes involved in the design and analysis of past experiments, but extended in this study to much longer distances as is required for future machines.

The technical challenges for making TBA's into realizable power sources lie in the dynamics of the drive-beam which must propagate over long distances. In particular, the beam-break-up (BBU) instability through a long multi-cavity RK-TBA is known to be severe. While BBU suppression techniques have been successfully demonstrated for a few cavities[15], a scenario with acceptable BBU control over many traveling-wave cavities must be constructed. Similarly, the longitudinal stability of the rf bunches over a multi-cavity TBA must also be demonstrated.

A detailed description on the new RK-TBA architecture has already been given[13], for the convenience of the following discussion, we briefly review some of the main features of the 1 TeV RK-TBA.

To generate an unloaded gradient of 100 MV/m in the high-gradient structures, the TBA
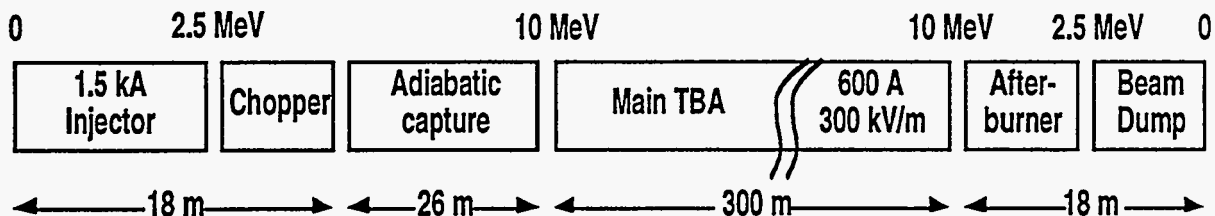
2

0	2.5 MeV		10 MeV		10 MeV	2.5 MeV	0
1.5 kA Injector	Chopper	Adiabatic capture	Main TBA	600 A 300 kV/m	After-burner	Beam Dump	

←——18 m——→ ←——26 m——→ ←——————300 m——————→ ←——18 m——→

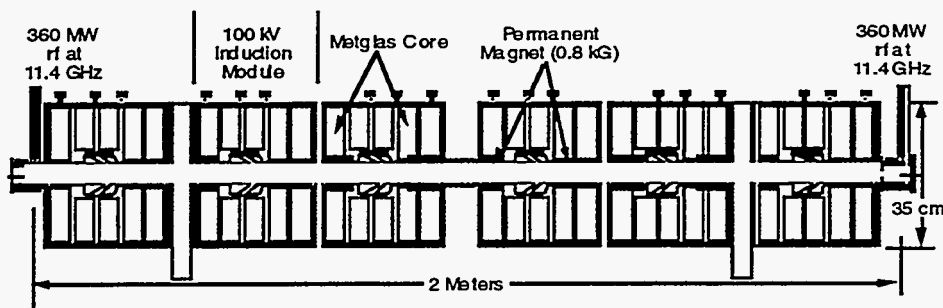**FIGURE 4.** Schematic of one RK-TBA unit.

FIGURE 5. 2-m module in the main TBA.

must supply 360 MW of rf power at 11.4 GHz every 2 meters. The output rf field is specified to have a 100 ns linear rise followed by 200 ns flat-top. To power a 15 km long collider (7.5 km for each arm), we propose an architecture with 50 RK-TBA units, operating at an average drive beam energy of 10 MeV, with an average current of 600 amps over the duration of the pulse, and a reacceleration gradient of 300 kV/m. Each unit would supply the rf power for 300 m of the high energy linac. A schematic of one RK-TBA unit is shown in Figure 4, and a layout of a 2-m module which is repeated 150 times in the main TBA is given in Figure 5.

The front end of each RK-TBA unit consists of a 1.5 kA injector, followed by an rf chopper at 2.5 MeV, and an 'adiabatic capture' unit in which the chopped beam (average current 600 A) is accelerated to 10 MeV and further bunched with idler cavities in preparation for injection into the main TBA. To enhance the efficiency of the TBA system, an 'afterburner' at the end of the main TBA continues to extract rf power through 12 successive output cavities before depositing the spent beam (average beam energy < 3 MeV) at the beam dump. The overall efficiency (drive-beam to rf) of each RK-TBA unit is calculated to be ~ 90%.

2. LONGITUDINAL BEAM DYNAMICS

Longitudinally, beams will debunch because of space-charge and rf-induced energy spread. To counter these debunching effects, the rf output cavities are inductively detuned. This is accomplished by making the phase velocity of the 3-cell traveling-wave structure (TWS) faster than the velocity of the particles (V_p = 1.33 c). The particle bunch lags behind the decelerating crest of the wave, and the energy loss becomes phase dependent, with the particles at the bunch tail losing the least energy. Kinematics lead to a 'catching up' of the tail with the bunch front and subsequent synchrotron oscillation in stable rf buckets.

We carried out numerical simulations using a code named "RKS" developed by Ryne and Yu[11] for studying the interaction of a charged particle beam with an electromagnetic wave in a relativistic klystron. The code solves self-consistently the single particle

3

equations of motion for the beam and the coupled circuit equations that govern cavity excitation and it includes the calculation of the space charge effect. It assumes a single dominant mode and cylindrical symmetry of its fields inside the cavity. To use the RKS code to study the inductive detuning cases, we generalized the analytic theory developed by Ryne and Yu[16] and obtained a more general matching condition formula[17] which is valid for the non-synchronism cases as well as for the synchronism case. This matching condition, once satisfied, will guarantee that the TWS propagates and amplifies only a forward traveling wave. The formula is given as follows

$$
\begin{aligned}
\omega_N &= \omega_v - \frac{V_g}{2L_p \cdot \sin(\alpha)} \left[\frac{\sin(N+1)\Delta^-/2}{\sin(N\Delta^-/2)} \cos \Delta^+/2) \right] \\
(Q_N)^{-1} &= \frac{V_g}{\omega_N L_p \cdot \sin(\alpha)} \left[\frac{\sin(N+1)\Delta^-/2}{\sin(N\Delta^-/2)} \sin(\Delta^+/2) \right]
\end{aligned}
\tag{1}
$$

where ω_N and Q_N denote, respectively, the eigenfrequency and the external quality factor of the last cell (output cell) of a N-cell TWS. ω_v denote the eigenfrequencies of the other N-1 cells in the TWS, which are assumed to be identical. L_p and V_g denote, respectively, the longitudinal dimension and the group velocity of a single cell. Also α and α' are, respectively, the phase advances of the wave field and the beam across one cell. In (1) we also have $\Delta^\pm = \alpha' \pm \alpha$ with Δ^- being defined as the so called detuning angle. Then $\Delta^- = 0$ corresponds to the synchronism case, while $\Delta^- \neq 0$ corresponds to the non-synchronism case and in particular $\Delta^- > 0$ corresponds to the inductive detuning case when the wave travels faster than the beam.

We have also derived in our theory a formula that quantifies the power extraction from the output cell of a N-cell TWS. The formula may be expressed as follows

$$
P_{out} = \Gamma(\Delta^-) \cdot \left\{ \frac{(I_{ind})^2}{4} \left(\frac{\omega L_p}{V_g} \right) [(\frac{R}{Q})/2] \cdot N(N+1) \right\}
\tag{2}
$$

where I_{ind} and R/Q denotes, respectively, the induced current and the shunt impedance of the structure. The coefficient $\Gamma(\Delta^-)$ is a function of the detuning angle Δ^- and it can be determined from the numerical simulations using the RKS code. Eq. (2) relates the power output P_{out} to the induced current, the detuning angle and also the cavity parameters; it is useful for cavity design.

In the following we present the results of our RKS simulation study on the "inductive detuning scheme" and several other issues related to the longitudinal dynamics of the drive beam in a 1 TeV RK-TBA.

2.1. RK-TBA with inductively detuned TWS's

Figure 6 presents the output power from each of 150 TWS's in the main TBA section for both a successful detuning case and a corresponding synchronism case. It is seen that when the cavities are properly detuned, the rf bucket can be maintained stably and output power can be sustained at the desired level (~360 MW) for all the 150 extraction cavities. In contrast, cavities with no inductive detuning are shown to result in sharp decline of the output power level even after a few cavities, due to the space charge debunching.

The synchronism case in Figure 6 consists of conventional 3-cell TWS's operating at
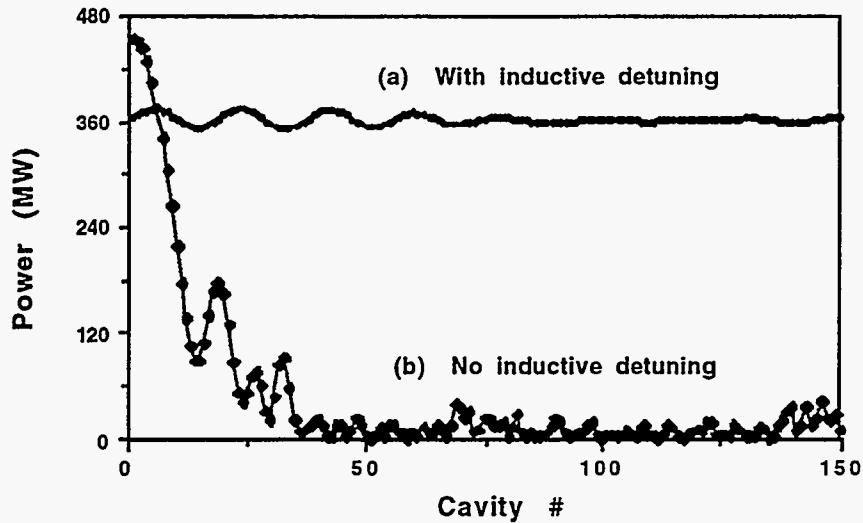
FIGURE 6. Power extraction from 150-cavities in one unit of RK-TBA.

TM_{010} mode that has $2\pi/3$ phase advance per cell. In the inductively detuned case the operating detuning angle is $30°$ the cavity is therefore operating at TM_{010} mode that has $\pi/2$ phase advance per cell. The longitudinal dimension of each cell is the same in the two cases while the transverse dimensions are varied. *URMEL* and *MAFIA* codes were used for detailed cavity design. Cavity parameters listed in Table 1 were obtained from these code studies. Also Figures 7(a) and 7(b) are, respectively, cavity outer radius vs. cavity inner radius and shunt impedance, group velocity vs. cavity inner radius, for the $\pi/2$ TM_{010} mode.

TABLE 1. Parameters Related to the Inductive Detuning Case

|	
Drive frequency	11.424 GHz
Operating Mode	TM_{010}
Phase shift per cell	$90°$
Wave length	2.626 cm
Phase velocity	1.33 c
Number of cells	3
Group velocity (V_g)	0.28 c
Shunt impedance per cell (R/Q)	13.5 (Ω)
Eigenfrequency for the first 2 cells	11.424 GHz
Eigenfrequency for the 3rd cell	11.666 GHz
Wall-dissipation quality factor	7000
External quality factor for the 3rd cell	6.5
Aperture inner radius (a)	8 mm
Aperture outer radius (b)	12.5 mm
Iris thickness	2.5 mm
Longitudinal dimension of each cell	8.754 mm
Beam energy	10 MeV
Beam current (average)	600 A
Bunch length	0.51 cm
Beam radius (rms)	2.5 mm
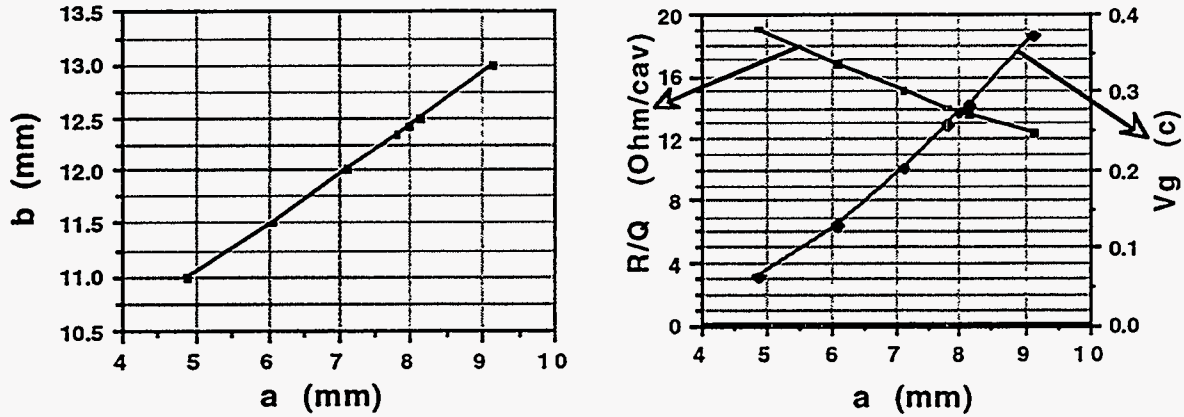
FIGURE 7. For $\pi/2$ TM_{010} mode: (a) cavity outer radius, b, vs. inner radius, a; (b) shunt impedance, R/Q, and group velocity, V_g, vs. cavity inner radius.
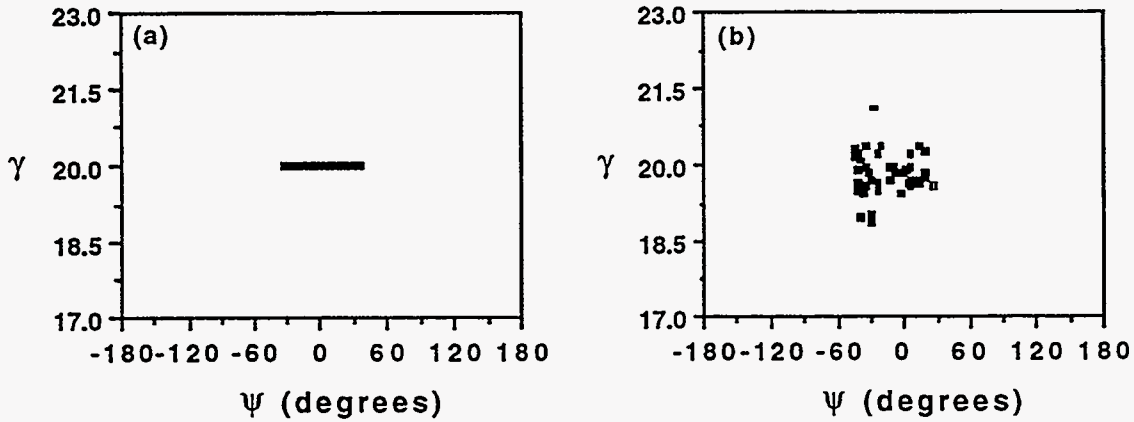

FIGURE 8. Phase distribution of a beam bucket for the inductive detuning case in Fig. 6: (a) Just before the 1st TWS; (b) after the 110th TWS and 2 m reacceleration.

Figures 8(a) and 8(b) are the longitudinal phase distribution of a beam bucket for the inductive detuning case in Fig. 6 just before the 1st TWS and after the 110th TWS, respectively. It is seen that after 110 extraction cavities the beam bucket maintains the initial bunch length, ~ 70° (the wave length is 360°). It is also noted that the bucket has a large energy spread, 10 ~ 15%, which provides strong Landau damping and can drastically reduce the transverse instability (BBU) in the induction machine, as will be discussed in Section 3.2.

A key feature for RK-TBA design is the time it takes for rf field in a cavity to reach an equilibrium state. Figure 9 presents the time dependences of output power at the 50th, 100th and 150th extraction cavities for the inductive detuning case in Fig. 6. It shows that in about 15 ns the rf fields in all the cavities reach their equilibrium states. This indicates that erosion of the beam head, due to the cavity filling process, is not serious. The short time to reach equilibrium is a result of the low Q and high V_g.

To sustain the level of output power throughout the main TBA the extraction cavities need to have enough detuning. Figures 10 shows that when the detuning angle is somewhat bellow 30°, e.g. at 25°, the cavities are unable to sustain the level of output power throughout the whole 150 TWS's.
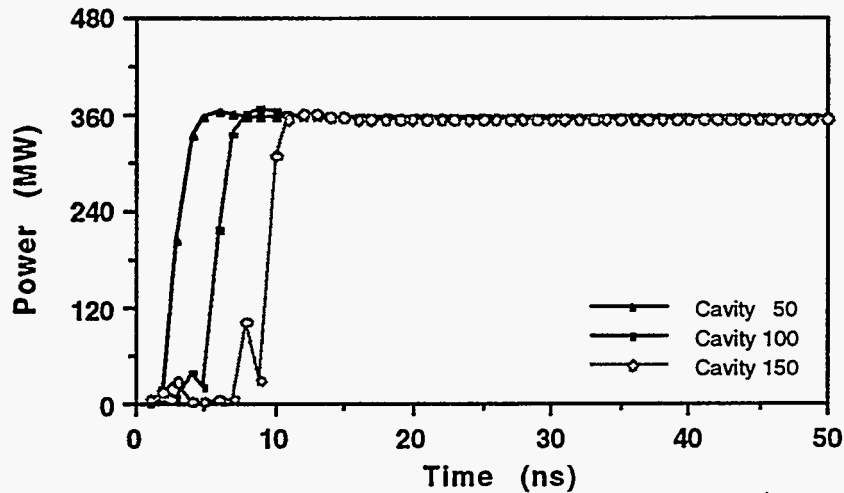
FIGURE 9. Time evolutions of output power at 3 TWS's for the detuning case in Fig. 5.
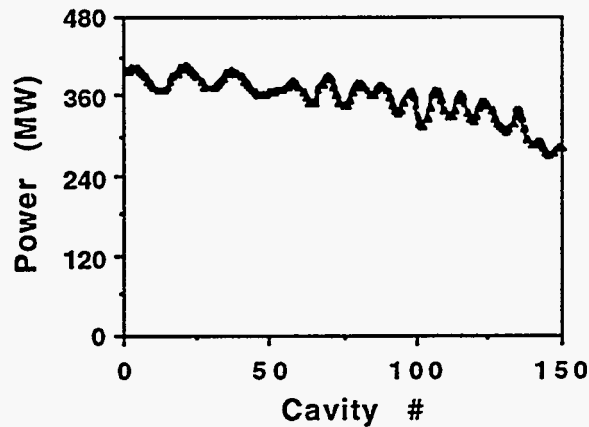
FIGURE 10 Power extraction from 150 cavities that are 25° inductively detunied (drive beam: 70° bunch length).

2.2. "Adiabatic Capture"

As we have learned from Section 2.1., the desired bunch length (0.51 cm or 70°) of the drive beam for stable propagation in the main TBA is about 1/5 of the distance between adjacent beam bunches (2.63 cm, or 360°). To help achieve high efficiency of beam energy to rf energy conversion, first is to produce relatively long bunches from a low energy DC beam, and then, compress the bunches with several properly spaced "idler cavities" (cavities with large detuning angles). During the same process the beam is also being accelerated by induction cells that are placed along the drift tubes between the "idler cavities". In this way we can obtain a train of beam bunches with desired energy and bunch length, and the loss of beam energy is minimum. A schematic of such this so-called "adiabatic capture" scheme is given in Figure 11.

Figure 12 presents the evolutions of bunch length and kinetic energy of a beam bunch, that starts with 2.5 MeV kinetic energy and 240° bunch length, through a 26 m "adiabatic capture" section and results, finally, in the desired 10 MeV energy and 70° bunch length.
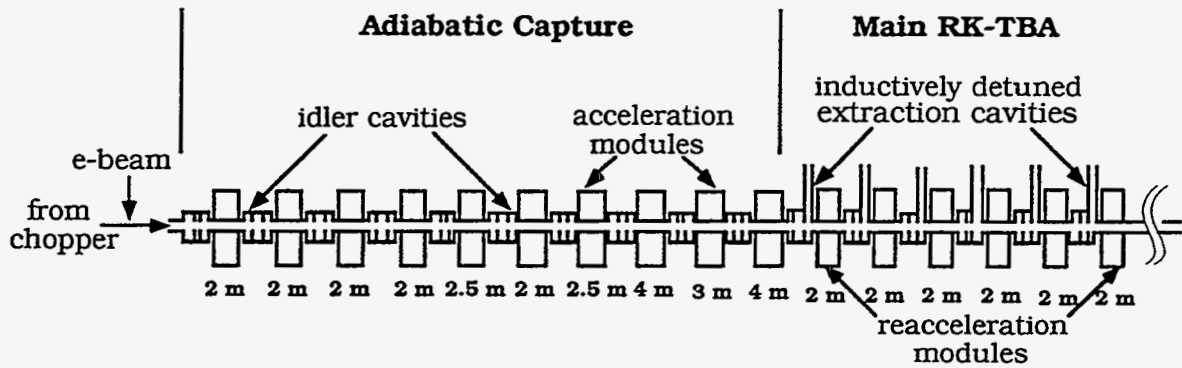
FIGURE 11. Schematic of "adiabatic capture" scheme.
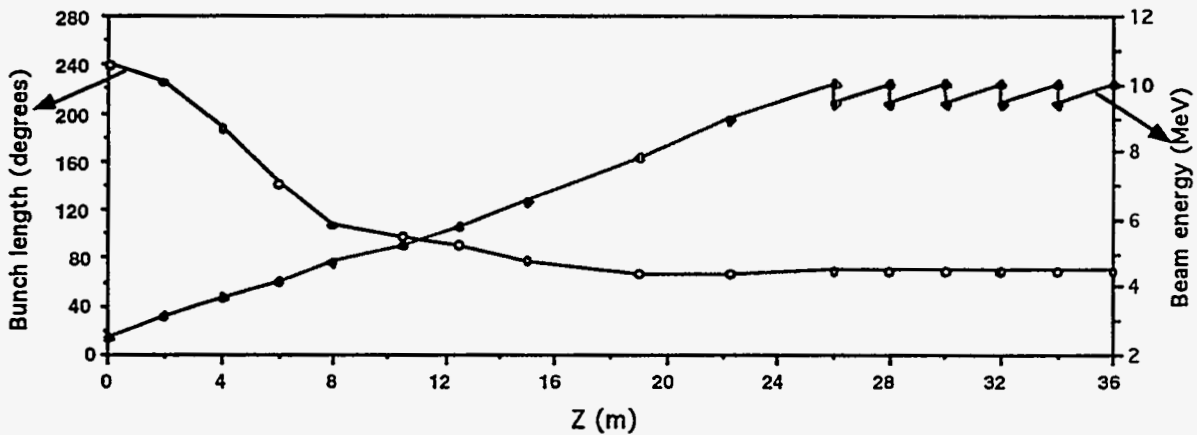
FIGURE 12. Evolutions of bunch length and kinetic energy of a beam bunch during the "adiabatic capture" process illustrated in Fig. 11.

Figures 13(a) and 13(b) are, respectively, phase distribution of the bunch before and after the adiabatic capture. It is noted that the bunched beam has about 10% energy spread which is consistent with the equilibrium rf bucket in the main TBA section. The chief parameters associated with this process are given in Table 2 in which L denotes the distance from the 1st cavity, $\Delta\Phi$ denotes the bunch length in degrees and E_k denotes the kinetic energy of the beam. All the "idler cavities" used are 3-cell TWS's with 70° detuning.

FIGURE 13. Phase space distribution of the beam bunch in Fig. 11: (a) before the "adiabatic capture" process; (b) after the "adiabatic capture" process.

8

TABLE 2. Some Parameters for "Adiabatic Capture" (2.5 MeV and 240º)

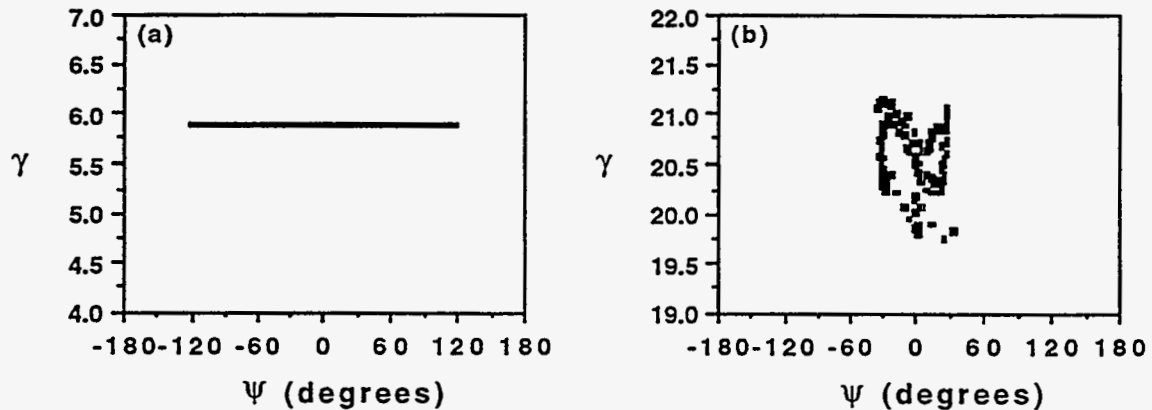| TWS #	V_g (c)	L (m)	$\Delta\Phi$ (º)	E_k (MeV)
1	0.20	2.0	226.0	3.12
2	0.20	4.0	187.0	3.63
3	0.20	6.0	140.9	4.14
4	0.18	8.0	106.8	4.70
5	0.18	10.5	97.7	5.26
6	0.16	12.5	89.8	5.77
7	0.16	15.0	78.1	6.49
8	0.15	19.0	65.7	8.43
9	0.14	22.0	66.3	8.94
10	0.14	26.0	70.0	10.00

2.3. The Chopper

As has been mentioned in the previous section, in our RK-TBA design, after the drive beam is emitted from the injector it needs first to go through a chopper to generate a train of beam bunches of certain bunch length before entering the "adiabatic capture" section to acquire further bunching and acceleration. A layout of chopper mechanism[18,19] is shown in Figure 14 in which the modulator of the chopper is a 5.7 GHz chopping system designed to produce a train of beam bunches with a period corresponding to 11.4 GHz from an initial uniform beam.

We simulated the chopper operation with 2-1/2 dimension RKS code, and then used the obtained more realistic distribution of the beam bunch as the initial condition for the RKS simulation and re-examined the corresponding "adiabatic capture" process and the main TBA transport. The result is given in Figure 15. Although this result is for an initial 5 MeV beam and the bunches that exit the chopper span 180º, we believe that the final conclusion is the same. It is seen in Fig. 15 that the level of the output power remains at 360 MW throughout the entire main TBA section with fluctuation less than 8.5%. The cavity parameters associated with the main TBA section are the same as those given in Section 2.1.
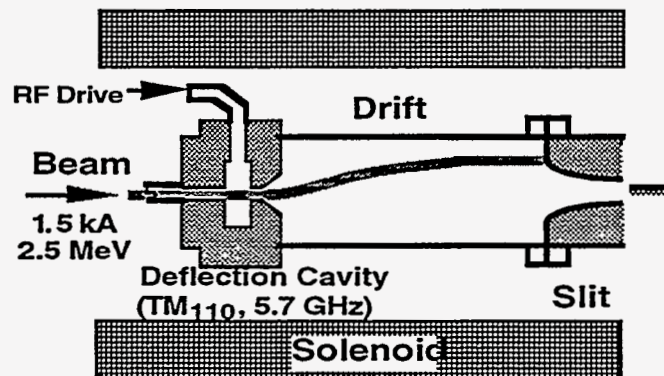

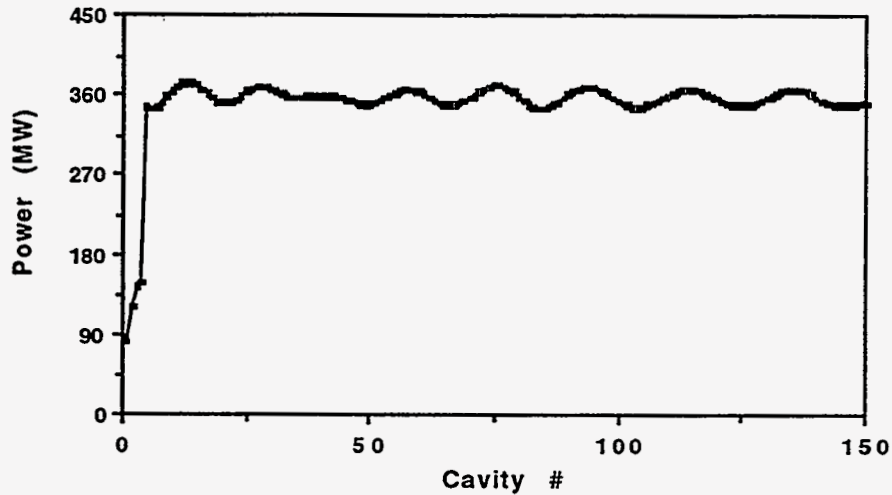
FIG.14. Layout of chopper mechanism.

FIGURE15. Evolution of output power from the adiabatic capture section to the main TBA section with the beam bunches coming out of the chopper as the initial condition.

2.4. After-burner

The electron beam that comes out of the main RK-TBA is still a beam with about 9.4 MeV kinetic energy and 600 A average current. To make the most use of this amount of energy, and to further enhance the beam-to-rf efficiency, we have another section called the "after-burner" which consists of a dozen or so TWS's that are just like, or similar to, those used in the main TBA. In the "after-burner" section the cavities are designed and arranged in such a way that each of them takes out also about 360 MW power from the beam. As for a single period, compared to the main TBA section, in the "after-burner" section: (1) there is no reacceleration, and (2) the distance between two adjacent cavities is adjustable so that the cavities can be placed at positions where the rf current of the drive beam is relatively stable

TABLE 3. Some Parameters for "After-Burner"

TWS #	V_g (c)	L_s (m)*	P_{out} (MW)	E_k (MeV)
1	0.28		363.	8.80
2	0.28	1.50	365.	8.19
3	0.28	1.40	365.	7.58
4	0.28	1.30	362.	6.98
5	0.27	1.30	366.	6.37
6	0.27	0.80	357.	5.77
7	0.26	0.60	362.	5.17
8	0.26	0.50	355.	4.58
9	0.25	0.60	361.	3.98
10	0.24	0.70	361.	3.37
11	0.22	0.65	369.	2.76
12	0.22	0.45	358.	2.16

* Distance from the last cavity. (Initial energy spread $\Delta\gamma/\gamma = 15.\%$)

and about the same as it is in the main TBA section. In addition to the efficiency enhancement, another benefit of the "after-burner" scheme is that it lowers the final energy of the beam considerably, and therefore, makes the disposal of the spent beam much easier.

We have carried out RKS simulation on the "after-burner" section in which 12 TWS's with 30° detuning are properly arranged. The results and some related parameters are given in Table 3. It is seen in Table 3 that with the proper choices of the group velocities (V_g) and the spacing (L_s), each of the cavities is able to extract about 360 MW from the beam and the final energy of the beam is around 2.2 MeV. This means a 77% beam to rf efficiency for this section, and therefore, raises the overall drive beam to rf conversion of each RK-TBA unit from 87% to 94%.

3. TRANSVERSE BEAM DYNAMICS

Transverse beam instabilities due to the excitation of higher order modes in the various structures comprising the relativistic klystron has been identified as a major issue in the design of a RK-TBA[15]. The narrow aperture and high average current of the relativistic klystron accentuates the problem. As will be discussed below, there are two structural components that contribute to the transverse instability. The output structure with a 1.6 cm aperture has a transverse mode near 14 GHz that interacts strongly with the beam (high frequency instability) and the induction module with an aperture of 5.0 cm has a trapped dipole mode around 2 to 5 GHz (low frequency instability).

Two primary mechanisms for the transverse instability are associated with the RK-TBA system. The individual induction cells and output structures are assumed to be electromagnetically isolated and the growth of the transverse instability is due to cumulative beam breakup (BBU). The output structures each comprise several electromagnetically coupled cavities which are subject to the regenerative mechanism for transverse instability.

There has been extensive analytical work accomplished for the cumulative BBU[20], but analytic study for the regenerative BBU proves to be more difficult and numerical simulation is needed to quantify the process. A computer code named "OMICE" was recently developed by Houck at LLNL[12] to numerically investigate the transverse instability in microwave structures consisting of electromagnetically coupled cavities. The OMICE Code assumes a single dipole cavity mode is dominant and the y-polarization of the magnetic field in the nth cavity can be expressed as

$$\vec{B}_n(\vec{r},t) = b_n(t)\, \vec{\xi}_n(\vec{r})\, e^{i\omega t}, \tag{3}$$

where $\vec{\xi}_n$ denotes an eigenmode with eigenfrequency ω_n and ω denotes a characteristic frequency of the generator assumed near the transverse instability resonance. It is possible to show that the excitation amplitudes b_n are governed by the following circuit equations:

$$\frac{\partial^2 b_n}{\partial t^2} + \left(\frac{\omega_n}{Q_n} - 2i\omega\right)\frac{\partial b_n}{\partial t} + \left(\omega_n^2 - \omega^2 - \frac{i\omega\omega_n}{Q_n}\right)b_n =$$
$$K_n^{n-1}\, b_{n-1} + K_n^{n+1}\, b_{n+1} + \frac{i\,\omega\,\omega_n^3}{\varepsilon\, c^2}\left(\frac{Z_\perp}{Q}\right)_n Ix\, e^{-i(\omega t + \phi_n)}, \tag{4}$$

where Q_n denotes the quality factor of the nth cavity, $K_n^{n\pm1}$ denotes the coupling of the n and n±1 cavities, I is the current, x is the transverse displacement of the beam centroid in the x direction from the center line, ϕ_n is the phase advance of the field across the nth cavity, and $Z_\perp/Q$ is the transverse shunt impedance. A second equation is used for the x-polarization

11

field, and single particle equations of motion in the x and y directions are included. In the OMICE code, RF structures are treated as separate entities with specific rf properties, and the electromagnetic coupling of cavities allows the effect of regenerative BBU to be included in the analysis besides the cumulative BBU.

3.1. High-Frequency Instability (RK-TWS's)

There is one 3-cell, traveling-wave, output structure (TWS) every two meters through the RK-TBA. The contribution of the output structures to the transverse instability of the beam is greater than that of the induction cell gaps. This is due to several reasons: (i) the output structure has a smaller aperture to obtain the desired longitudinal shunt impedance; (ii) damping of the higher order modes must not affect the fundamental mode used for power extraction, and (iii) the three cells comprising the TWS are electromagnetically coupled, therefore, within the TWS, the regenerative BBU mechanism will increase the strength of the higher order modes.

Previous study[10] has indicated that even with modest de-Q-ing, appropriate choice of cavity geometry (reducing $Z_\perp/Q$), staggered tuning and inclusion of the Landau damping mechanism, the growth in the transverse instability is still excessive for an efficient RK-TBA. Past experiences in the design of induction accelerators showed that a growth of 4 to 5 e-folds is tolerable in the transverse instability[21,22]. In the context of our current design, we can tolerate a transverse beam displacement of 4 to 5 e-fold over the 300 meter system, or 150 TWS's. In order to keep BBU to this level, we need to minimize or suppress excitation of the higher order (transverse) modes in the TWS's. The "betatron node scheme"[7] appears to be a promising means to achieve this goal. In the following, we examine the effect of this scheme in suppressing the BBU in the context of our current design.

The OMICE code is used to model the growth of the BBU. For our analysis, we choose a set of base parameters that match engineering design objectives. A list of the pertinent variables, and their base values, is given in Table 4. We then use the code to model the time-dependent transverse behavior of one 300 ns pulse over the full 300 m length of a TBA beam line.

TABLE 4. Base Parameters for Simulated Traveling Wave Structures	
Transverse Mode	HEM_{110}
Frequency of Mode ω_0	14.1 GHz
Number of Cells/TWS	3
Electrical Length of Each Cell L_c	8.754 mm
Phase Advance/Cell ϕ	120°
Group Velocity V_g	0.25c
Q_{wall} (1st and 2nd cells)	7000
Typical Q_{damped}	15
$Z_\perp/Q$ for each cell	3
RF Current I	600 Amps
Pulse Length	300 ns
Beam Energy E_0	10 MeV
Quadrupole Field (B_{zo}) 'On-Node'	0.0812 T

3.1.1. The "Betatron Node Scheme"

The "betatron node scheme" is used to limit the growth in the transverse instability to an acceptable level. In this scheme, the betatron wavelength of the focusing system is set to correspond to the spacing of the TWS's, so that deflection of the beam passing through a TWS will not result in further transverse displacement of the beam at the following TWS. Since the energy transfer from the beam to the higher modes of the TWS is proportional to the transverse displacement of the beam in the cavity, the "betatron node" scheme minimizes the increase of energy in the higher order modes, and therefore, the growth of the transverse instability.

In Figure 16, we present two simulation results to demonstrate the effectiveness of the "betatron node" scheme. In the 'on-node' case (a), a quadrupole B-field value is chosen to give a betatron wavelength of 2 meters, the distance between any two adjacent TWS's in the main TBA. This places the betatron node at the center of each TWS; the integrated transverse displacement of the beam in each TWS is thus minimized, and the transverse kick due to the wake field is suppressed to an acceptable level. In the 'off-node' case (b), the B-field over-focuses by 11%, shortening the betatron wavelength accordingly. Thus, as the beam position increases in z, its betatron nodes fall short of the TWS by an increasing amount, resulting in the beam having a large off-axis displacement, and therefore, the BBU growth occurs at a much greater rate than in the 'on-node' case.

Note that focusing strength is not the issue here. A specific betatron frequency is necessary to keep the beam on-node. Figure 17 shows the sensitivity of the transverse growth of the beam centroid after passing through 150 TWS's to the quadrupole B-field value (B is normalized to B_0, the value that corresponds to an 'on-node' betatron wavelength). The area below the 'tolerable growth' line is the region of operational stability for the system. As can be seen, a deviation from the correct B-field strength in either direction even as small as 0.5% will result in excessive growth. Such a tolerance level can hardly be achieved given the design precision of quadrupole magnets, but could be achieved by measuring, and properly adjusting, the betatron wavelength.
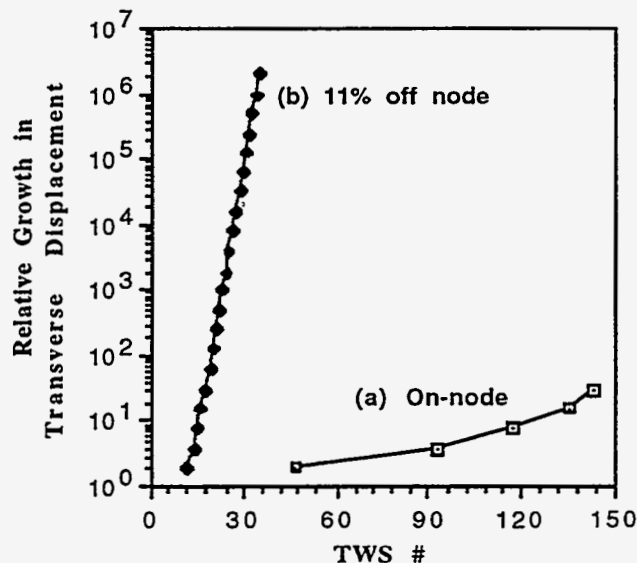

FIGURE16. Relative beam centroid displacement vs. the number of TWS's the beam traverses: (a) on-node; (b) off-node.
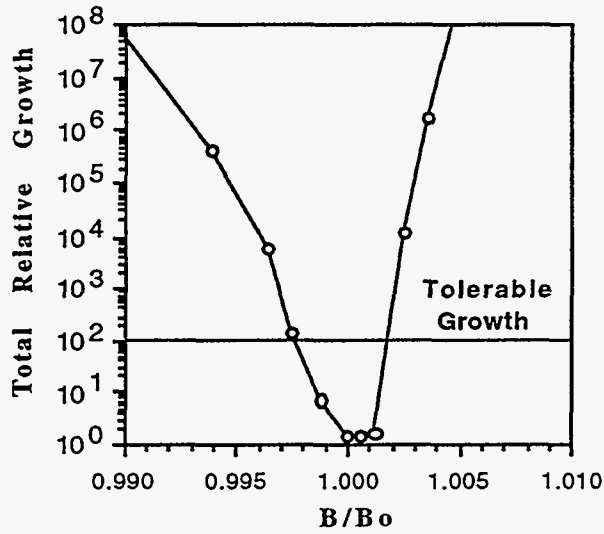
13

FIGURE17. Total relative growth after 150 TWS's vs. B-field.

3.1.2. Landau Damping

It is known that a finite energy spread on the beam bunches can reduce or even suppress the transverse growth of the beam displacement due to the BBU (Landau damping). It is noted in our study of the longitudinal dynamics in Section 2 that the equilibrium "rf-bucket" for the main RK-TBA has a finite energy spread (about 10~15%). This energy spread provides a natural Landau damping mechanism. When such an energy spread is introduced on the pulse, there is a spread in betatron wavelengths about the optimum value of 2 meters; most of the beam will thus be slightly over- or under-focused at all times. As a result, the "betatron node" scheme will not be as effective, but lower instability growth will occur when operating at a non-optimum *B*-field. It is seen from Figure 18 that, as expected, Landau damping does significantly reduce the growth in the transverse instability for most values of the focusing field off-optimum. However, the energy spread resulted in higher
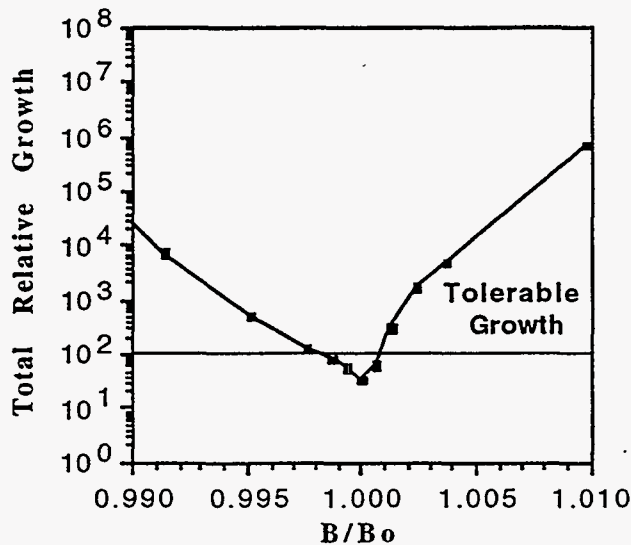

FIGURE18. Total growth after 150 TWS's vs. B-field with 15% Landau damping.

14

growth near the optimum, and the tolerance for acceptable growth does not improve.

It is clear from Figs. 17 and 18 that the "betatron node" scheme allows us to approach our goal of suppressing BBU to 4-5 e-fold, and Landau damping blunts the extreme sensitivity of the node scheme to fluctuations in the B field. However, additional measures are still needed to keep the region of operational stability large enough for a viable design. If required, we can achieve this goal by reducing the effective impedance ($Z_\perp/Q$) and/or Q factors of the higher order mode for the TWS's, and thereby, lowering the overall growth of the BBU.

3.1.3. Effective Impedance and Q Factor

The parameters that are most easily controlled in designs are the Q values of individual cells, and with somewhat more difficulty, the effective $Z_\perp/Q$ of the output structure. The Q of an RF cell can be reduced by (i) increasing the aperture to permit propagation of electromagnetic energy from the cell, (ii) adding absorbing material to the cell, and (iii) making external ports in the cell walls to couple out energy. The last option has the least interference with the fundamental mode and has been used successfully in the experimental program at LLNL[23,24].

The possibility of regenerative BBU within each TWS limits the applicability of the well-understood cumulative BBU theory[25,26]. However, by varying the Q and $Z_\perp/Q$ of the output structure cells in our simulations, we demonstrated, respectively, in Figures 19(a) and 19(b) the exponential dependence of the asymptotic BBU growth, $e^{\Gamma z}$, with respect to each of the above two parameters.

Next we tested the sensitivity of the BBU growth to different sets of Q values for the 3-cell TWS's. The results are given in Table 5 for 4 realistic sets of Q values. The first entry in Table 5 reflects the 'standard parameters' used to obtain the stability graph in Fig. 17. It is seen that lowering the Q for the 3rd cell from its base value even slightly will reduce the minimum relative growth by a significant margin (e.g., reducing Q_3 from 15 to 12 cuts the total BBU growth by half), and also applying de-Q-ing to the 1st cell in addition to the 3rd one can suppress the total BBU growth over 150 TWS's to less than 2 e-folds level. The exponential dependence of BBU growth on Q implies that this will result in an overall relative growth reduction, and therefore, increase the 'region of stability' to a satisfactory level.
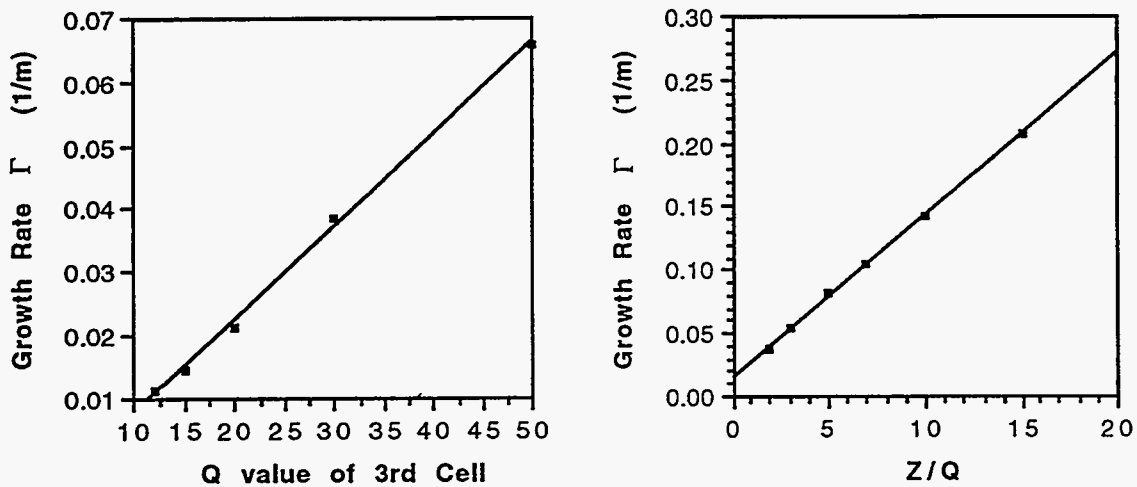

FIGURE19. Asymptotic BBU growth rate Γ verses: (a) Q of the 3rd cell; (b) $Z_\perp/Q$ per cell.

TABLE 5. Relative BBU Growth Over 150 TWS's for Different de-Q-ing Schemes			
Q (cell 1)	**Q (cell 2)**	**Q (cell 3)**	**Relative Growth**
7000	7000	15	32.7
7000	7000	12	16.3
15	7000	15	9.1
12	7000	12	4.4

3.2. Low-Frequency Instability (Induction Modules)

A. Problem Description

There are three induction modules per meter in the relativistic klystron (see Fig. 5). Although considerable damping can be accomplished by the insertion of absorbing material, design constraints imposed by the high surface electrical fields and vacuum requirements preclude complete damping of higher order modes. Modeling the module as a cylindrical resonator with an impedance boundary condition on the outer wall[27] and assuming an optimum design, the transverse impedance, $Z_{\perp 1}$, will be on the order of 4,000 Ω/m. In the context of our current design, we can tolerate a transverse beam displacement of 4 to 5 e-fold over the 300 meter system, or 150 TWS's. Then with $\lambda_\beta = 2$ m, I = 600 A, and Lg = 0.333 m, it is estimated the maximum tolerable transverse impedance of the module: $Z_{\perp 1}$ = 573 Ω/m. Thus, additional measures are needed to suppress the transverse instability.

B. Suppression Techniques

Several methods, such as (1) the addition of absorbing material, (2) de-Q-ing, (3) staggered tuning and (4) the "betatron node" scheme, have been examined and found either not effective or impractical for this case.

The most promising technique for suppressing such transverse instability is Landau damping. As we learned in Sec. 2, to maintain longitudinal equilibrium, a ±7.5% spread in beam energy over the microbunch is anticipated. Using analytic theory[19] it can then be
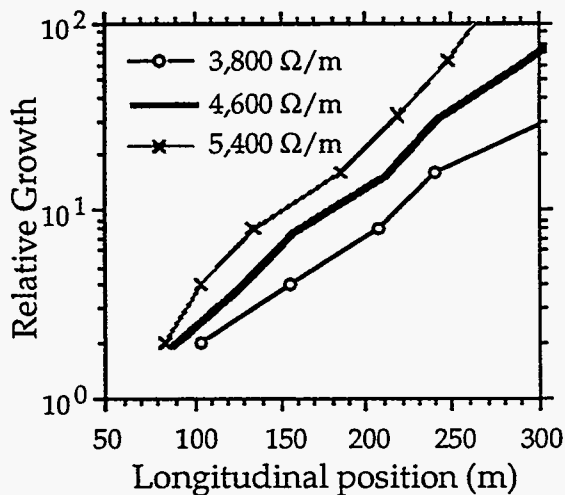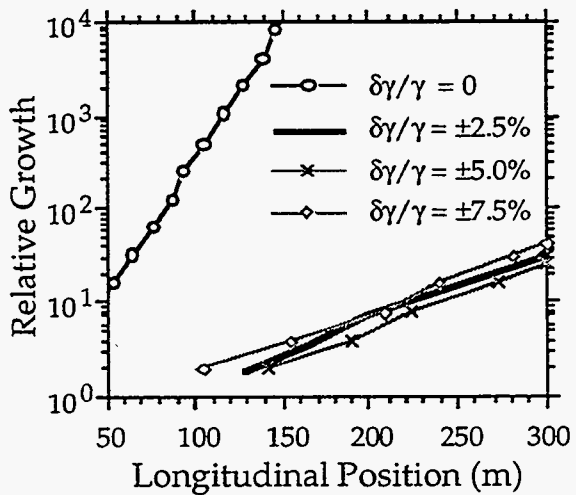
FIGURE 20. Growth for different $Z_{\perp 1}$.

FIGURE 21. Growth for different $\delta\gamma$.

found that for total suppression by Landau damping the estimated maximum transverse impedance, $Z_{\perp 1}$, is 5,178 Ω/m.

C. Results of Numerical Analysis

The OMICE code was again used to model the growth of the transverse instability. Figure 20 presents the relative growth in transverse displacement of the beam centroid from the axis as a function of distance along the axis. Three different cases are shown for $Z_{\perp 1}$ equals 3,800 Ω/m, 4,600 Ω/m, and 5,400 Ω/m to verify that the growth factor is proportional to $Z_{\perp 1}$. Table 6 lists input parameters used in the OMICE code. The "seed" perturbation for exciting the instability was a sinusoidal oscillation of the centroid's transverse displacement at the instability frequency. Additional simulations were performed for a transverse resonance of 2 GHz, also to verify scaling, and no significant differences were noted. The effect of Landau damping is shown in Figure 21 for $Z_{\perp 1}$ equals 4,000 Ω/m and energy spreads from zero to ±7.5%.

The relative growth rates in Fig. 20 scale linearly with $Z_{\perp 1}$ as predicted by the theory on the cumulative BBU[26]. In Fig. 21, the growth rate for the case of no energy spread agrees to within 10% of the value predicted by theory. For finite energy spread cases, the theory[28] predicts relative growth rates of 0.09, 0.03, and 0.0 for $\delta\gamma/\gamma = \pm$ 2.5%, 5% and 7.5%, respectively. The numerical results in Fig. 21 show that all the relative growth rates with energy variation are about 0.02. There are several possible reasons for this discrepancy between analytical and numerical results. The results are dependent on the energy distribution and this is handled differently in the two cases. The perturbation "seed" used in the numerical work is suppressed by phase mixing when there is an energy variation. Also, the numeric model represents a finite number of particle orbits. The orbits will eventually become in phase again. This is the explanation for the increase in growth for $\delta\gamma/\gamma = \pm 7.5\%$ vs. that with ± 5.0%.

The conclusions from the numerical modeling are that the instability growth rate is conservative for energy spreads of ±7.5% and acceptable for $Z_{\perp 1}$ less than or equal to 4,600 Ω/m.

TABLE 6. Input Parameters for OMICE Code

BBU Frequency	3.0 GHz
$Z_{\perp 1}$ (Ω/m)	3,800/4,600/5,400
$Z_{\perp}/Q$ (Ω)	30.2/36.6/43.0
Cell Q	2
Gap Width	2.5 cm
Average Beam Energy	10 MeV
$\Delta\gamma/\gamma$ ($\Delta\gamma = \gamma_{max} - \gamma_{min}$)	15%
Current (dc component)	0 – 600 A in the 1st 100 ns 600 A "flat top" in the next 200 ns
Focusing System	Quadrapole - 2m period
Time Step	1/600 ns

4. SUMMARY

A. Longitudinal beam dynamics

It is demonstrated in this study that the "inductive detuning" scheme is able to contain space charge debunching effect on the drive beam and achieve stable power output at the desired level for 150 extraction cavities in the 1 TeV RK-TBA; also the beam bunches desired by the RK-TBA can be efficiently obtained by first chopping an initially uniform beam of low energy into a train of beam bunches with modest length and then bunching and accelerating these bunches into tight bunches at the operating energy of the drive beam. It is also found that the "after-burner" scheme can be implemented in our RK-TBA design for efficiency enhancement.

In the future we will carry out 2-1/2 dimension RKS simulations to investigate, and if necessary compensate, a potential transverse defocusing effect due to the rf electric field in the output structures.

B. Transverse beam dynamics

The overall conclusion is that the primary cause of the BBU in the 1 TeV RK-TBA is the output structures. The "betatron node" scheme is, in principle, very effective in reducing the growth of BBU, and when combined with sufficient de-Q-ing and/or optimum cavity design (minimizing $Z_\perp/Q$) appears to be a promising means for controlling the high frequency instability caused by these structures. The lower frequency instability of the induction cell gaps will be adequately suppressed by Landau damping resulting from the anticipated energy spread in the equilibrium rf buckets.

Further studies are needed to determine the affect of different perturbation "seeds" on the initial growth of the instability, and to understand the sensitivity of the "betatron node" scheme to head-to-tail energy variation over the beam pulse. Preliminary investigation is that systematic errors in the beam energy, focusing field strength, and/or output structure spacing must be avoided as they will greatly reduce the effectiveness of the "betatron node" scheme, causing unacceptable growth in the BBU; random variation about the desired operating parameters is not serious, and, in the case of a transverse energy spread, can be beneficial. Feedback schemes, to control systematic errors in focusing fields and average beam energy, need to be incorporated in the modeling.

ACKNOWLEDGMENTS

REFERENCES

1. Sessler, A. M., "The free-electron laser as a power source for a high gradient accelerating structure", *Workshop on Laser Acceleration of Particles*, NY, AIP Conference Proceedings **91**, 1982, pp. 154.
2. Sessler, A. M. and Yu, S. S., "Relativistic Klystron Two-Beam Accelerator," *Phys. Rev. Lett.*, **58**, No. **23**, 2439–2442 (1987).
3. Sessler, A. M., Sternbach, E., and Wurtele, J. S., "A New Version of a Free Electron Laser Two-Beam Accelerator", *Nucl. Inst. Method in Phys. Res.*, B**40/41**, 1064 (1989).

4. Sessler, A. M., Whittum, D. H., Wurtele, J. S., Sharp, W. M. and Makowski, M. A., "Standing-wave free-electron laser two-beam accelerator", *Nucl. Inst. Method in Phys. Res.*, A **306**, 592 (1991).
5. Kim, J. S., Henke, H., Sessler, A. M. and Sharp, W. M., "The Standing Wave FEL/TBA: Realistic Cavity Geometry and Energy Extraction", in *Proceedings of 1993 Particle Accelerator Conference*, Vol 4, 1993, pp. 2593.
6. Wang, C. B., "Simulation analysis of the effect of beam pipes and multi-mode competition in the standing-wave free-electron laser two-beam accelerator", *Nucl. Inst. Method in Phys. Res.*, A **346**, 416 (1994).
7. Li, H., Houck, T. L., Yu, S. S., and Goffeney, N., "Design Consideration of Relativistic Klystron Two-Beam Accelerator for Suppression of Beam-Breakup," *SPIE Proceedings* Vol. **2154-10**, 1994.
8. Orzechowski, T. J., et al, *Phys. Rev. Lett.* **57**, 2172 (1986).
9. Allen, M. A., et al, *Phys. Rev. Lett.* **63**, 2472 (1989).
10. Westenskow, G. A. and Houck, T. L., "Results of the Reacceleration Experiment: Experimental Study of the Relativistic Klystron Two-Beam Accelerator Concept," presented at the 10th International Conference on High Power Particles Beams, San Diego, CA, June 20-24, 1994, to be published in the Proceedings.
11. Ryne, R. D. and Yu, S. S., "Relativistic Klystron Simulations Using RKTW2D," in *Proceedings of the Conference on Linear Accelerator,* 1990, pp. 177.
12. Houck, T. L., Westenskow, G. A. and Yu, S. S., "BBU Code Development for High-Power Microwave Generators," in *Proceedings of the Conference on Linear Accelerator,* 1992, pp. 495-497.
13. Yu, S., et al., "Relativistic Klystron Two-Beam Accelerator As A Power Source For A 1 TeV Next Linear Collider – A Systems Study", presented at 17th Int'l LINAC Conf., Japan, August 22-26, 1994, to be published in the Proceedings.
14 Yu, S., Deadrick, F., Goffeney, N., Henestroza, E., Houck, T., Li, H., Peters, C., Reginato, L., Sessler, A., Vanecek, D. and Westenskow, G., "Relativistic Klystron Two-Beam Accelerator As A Power Source For A 1 TeV Next Linear Collider", preliminary design report, LBL, Berkeley, CA, September, 1994.
15. Houck, T. L., "Design Study of a Microwave Driver for a Relativistic Klystron Two-Beam Accelerator", *Proc. PAC*, 1993, pp. 2590.
16. Ryne, R. D. and Yu, S. S., "Using Traveling Wave Structures to Extract Power From Relativistic Klystrons," in *Proceedings of the Conference on Linear Accelerator,* 1990, pp. 180.
17 Li, H., and Yu, S. S., "Theory for Inductively Detuned Traveling Wave Structures", in preparation for publication.
18. Haimson, J. and Mecklenburg, B., *Report No. HRC-774, Haimson Research Corporation*, Palo Alto, CA, 1988.
19. Houck, T. L. and Westenskow, G. A., "Status of the Choppertron Experiments," in *Proceedings of the 16th Int'l LINAC Conf.,* 1992, pp. 498-500.
20. Lau, Y. Y., "Classification of Beam Breakup Instabilities in Linear Accelerators," *Phys. Rev. Lett.* **63**, 1141 (1989).
21. Kapetanakos, C.A. and Sprangle, P., "Ultra-high-current electron induction accelerators," *Physics Today* **38**, 58 (1985).
22. Clark, J., et. al., "Design and Initial Operation of the ETA-II Induction Accelerator," in *Proceedings of the 14 International LINAC Conf.*, 1988, pp. 19-23.
23. Haimson, J. and Mecklenburg, B., "Suppression of beam induced pulse shortening modes in high power RF generator and TW output structures," *SPIE Symposium on Intense Microwave and Particle Beams III Proceedings* Vol. **1629-71** 209 (1992).
24. Houck, T. L. and Westenskow, G. A., *Proc. 16th International Linac Conf.*, Ottawa, Ontario, Canada, Aug. 23-28, 1992, pp. 495- 497.
25. Panofsky, W. K. H. and Bander, M., "Asymptotic Theory of Beam Break-up in Linear Accelerators," *Rev. Sci. Instr.* **39**, 206 (1968).

26. Neil, V. K., Hall, L. S. and Cooper, R. K., "Further Theoretical Studies of the Beam Breakup Instability," *Part. Acc.* **9**, 213 (1979)
27. Brigg, R. J., et. al., "Theoretical and Experimental Investigation of the Interaction Impedances and Q Values of the Accelerating Cells in the Advanced Test Accelerator," *Part. Acc.* **18**, 41 (1985).
28. Caporaso, G. J. and Cole, A. G., "High Current Electron Transport," in the *AIP Conference Proceedings* **249**, Volume Two, The Physics of Particle Accelerators, eds. M. Month and M. Dienes, (AIP, New York), 1992, pp.1678.